Optimal control of a Cope rearrangement by coupling the reaction path to a dissipative bath or a second active mode

A. Chenel, C. Meier, G. Dive, and M. Desouter-Lecomte

Articles you may be interested in

Incorporating a completely renormalized coupled cluster approach into a composite method for thermodynamic properties and reaction paths
J. Chem. Phys. **136**, 144109 (2012); 10.1063/1.3700801

Quantum optimal control of isomerization dynamics of a one-dimensional reaction-path model dominated by a competing dissociation channel
J. Chem. Phys. **131**, 044306 (2009); 10.1063/1.3185565

Geometry optimization based on linear response free energy with quantum mechanical/molecular mechanical method: Applications to Menshutkin-type and Claisen rearrangement reactions in aqueous solution
J. Chem. Phys. **126**, 144503 (2007); 10.1063/1.2715941

Generation of initial trajectories for transition path sampling of chemical reactions with ab initio molecular dynamics
J. Chem. Phys. **126**, 024110 (2007); 10.1063/1.2424712

The generator coordinate method for a reaction coordinate coupled to a harmonic oscillator bath
J. Chem. Phys. **109**, 4028 (1998); 10.1063/1.477002

Optimal control of a Cope rearrangement by coupling the reaction path to a dissipative bath or a second active mode

A. Chenel,[1] C. Meier,[2] G. Dive,[3] and M. Desouter-Lecomte[1,4]

[1]*Laboratoire de Chimie Physique, UMR 8000 and CNRS, Université Paris-Sud, F-91405 Orsay, France*
[2]*Laboratoire Collisions, Agrégats, Réactivité, UMR 5589, IRSAMC, Université Paul Sabatier,*
F-31062 Toulouse, France
[3]*Centre d'Ingéniérie des Protéines, Université de Liège, Sart Tilman, B6, B-4000 Liège, Belgium*
[4]*Département de Chimie, Université de Liège, Bât B6c, Sart Tilman, B4000 Liège, Belgium*

We compare the strategy found by the optimal control theory in a complex molecular system according to the active subspace coupled to the field. The model is the isomerization during a Cope rearrangement of Thiele's ester that is the most stable dimer obtained by the dimerization of methyl-cyclopentadienenylcarboxylate. The crudest partitioning consists in retaining in the active space only the reaction coordinate, coupled to a dissipative bath of harmonic oscillators which are not coupled to the field. The control then fights against dissipation by accelerating the passage across the transition region which is very wide and flat in a Cope reaction. This mechanism has been observed in our previous simulations [Chenel *et al.*, J. Phys. Chem. A **116**, 11273 (2012)]. We compare here, the response of the control field when the reaction path is coupled to a second active mode. Constraints on the integrated intensity and on the maximum amplitude of the fields are imposed limiting the control landscape. Then, optimum field from one-dimensional simulation cannot provide a very high yield. Better guess fields based on the two-dimensional model allow the control to exploit different mechanisms providing a high control yield. By coupling the reaction surface to a bath, we confirm the link between the robustness of the field against dissipation and the time spent in the delocalized states above the transition barrier. © 2015 AIP Publishing LLC. [http://dx.doi.org/10.1063/1.4905200]

I. INTRODUCTION

In recent years, quantum control[1–6] has been successfully demonstrated for a wide variety of systems from nuclear spins to atomic or molecular systems.[7] Sophisticated experimental techniques now succeed in shaping the control fields in different spectral ranges.[8–10] These designed laser pulses act as new photonic reagents to drive molecular processes. Numerous experiments with adaptive feedback control efficiently cover many applications even in the presence of complex environments: isomerization,[11–13] photodissociation,[14] cooling,[15] alignment[16] or quantum computing,[17] and electronic dynamics.[18] On the theoretical side, one major tool to design the control field is Optimal Control Theory (OCT).[19] Several numerical iterative methods have been developed to solve the optimization problems: the gradient ascent algorithms,[20] the Krotov method,[21] or the monotonic methods.[22–24] While the efficiency of the latter procedure has been proven for low dimensional quantum systems, this approach becomes more and more prohibitive when the system complexity increases, mainly in the density matrix formalism usually used in dissipative dynamics. Moreover, models for large polyatomic molecules are too simplified to correctly predict the fine interference pathways. The latter are very sensitive to weak variations of the potential energy or dipolar momentum surfaces. However, simulations remain crucial for deciphering the control mechanism, exploring new strategies and obtaining qualitative information. Therefore, in the simulations, it is currently assumed that a small number of degrees of freedom can be controlled separately from the remaining ones. This is justified if subsystems have frequencies well different from those of the discarded modes. This means that the corresponding time scale of the active subspace is different from that of the surrounding. Most of the OCT simulations have been carried out in a reduced one-dimensional[25–29] or two-dimensional[30–36] subspace. Coupling OCT with MCTDH (Multi Configuration Time Dependent Hartree) is a promising issue to increase the dimensionality.[34,37,38] Simulation of systems coupled to an environment is still more challenging and requires a detailed knowledge of the system-bath coupling. Control in open quantum systems has been treated in the Redfield,[39–43] Lindblad,[44–47] or non-Markovian formalisms.[48–52]

In recent work,[53,54] we have presented an OCT simulation of an isomerization in a one-dimensional reaction path model coupled to an environment described by a bath of harmonic oscillators. The example was the Cope rearrangement of Thiele's ester that is the most stable dimer obtained by the dimerization of methyl-cyclopentadienenylcarboxylate.[53] Coupling the reaction path with a bath which does not interact directly with the laser field was the first attempt to take into account the other modes. The auxiliary matrix formalism[55,56] was combined with OCT to design control fields in the presence of dissipation. Very high performance index was obtained with short pulses of 5 ps. The main result was that to fight decoherence, the optimum field drives the system in such a way that it minimizes the time spent in the delocalized

states above the transition barrier. The first question of the present work is to examine the robustness of fields optimized on a reaction path when a second degree of freedom strongly coupled with the field is included in the system. The relevance of a reduced space simulation in a molecular control has already been addressed in the case of the HCN isomerization.[57] As expected, replacing the one-dimensional (1D) reaction path by a two-dimensional (2D) model dramatically increases the state density, particularly in the case of a Cope rearrangement which is characterized by a very wide and flat transition region. Therefore, the pulses obtained in the previous work[54] are too short to control the process. We optimize longer pulses of 15 ps in a 1D model and take them as trial fields for the 2D control. In all the simulations, we compare fields with the same integrated intensity. We examine what is the fingerprint of the 1D-field in the 2D-field control. Then, in a second step, we search a control strategy directly inspired from the properties of the 2D model and we compare the control mechanisms. We also confirm from the 2D fields that a field reducing the time spent in the delocalized states is more robust against dissipation. Finally, we address a third question: does the supplementary mode act as a dissipative bath during the controlled dynamics? The paper is organized as follows: in Sec. II, we describe the system and particularly the two-dimensional model based on quantum chemistry computation, and the different reaction paths under study. Section III summarizes the formalism of the optimal control. The 1D and 2D simulations of the Cope rearrangement of Thiele's ester are presented in Sec. IV and the conclusions and outlooks are given in Sec. V.

II. TWO- AND ONE-DIMENSIONAL MODELS

The Cope rearrangement of the methyl-cyclopentadienyl carboxylate dimer is illustrated in Fig. 1. The electronic energies and dipole moments have been computed by the density functional theory (DFT) with the B3LYP functional,[58] as implemented in the Gaussian09 software,[59] using the double-ζ basis set 6-31G(d). The initial state ϕ_i is the ground vibrational state of Thiele's ester[60,61] which is the major species formed during the dimerization[53] (form (a) in Fig. 1). The control target ϕ_t is the stable isomer (form (c) in Fig. 1) with a higher energy of 0.45 eV. The control proceeds via the Cope transition state (TS) (form (b) in Fig. 1) at 1.16 eV above Thiele's ester minimum. The transition barrier is particularly wide leading to a vanishingly small tunneling effect. In the TS structure, the two cycles are bound by a single bond, $r_1 = 1.6$ Å, while two internuclear distances r_2 and r_3 forming the structures (a) or (b) are long ($r_2 = 2.7$ Å and $r_3 = 2.8$ Å). Thiele's ester is obtained by decreasing r_2 up to $r_2 = 1.6$ Å while r_3 increases to $r_3 = 3.5$ Å. On the other side, structure (c) exhibits the opposite behavior with the final values $r_2 = 3.4$ Å and $r_3 = 1.6$ Å. Starting from the TS, Figure 1 shows in dashed line the two branches of the IRC (Intrinsic Reaction Coordinate) computed in mass-weighted coordinates. It is denoted RP0. The branch towards the product (structure (c)) nearly reaches the minimum by stopping at $r_2 = 3.45$ Å and $r_3 = 1.63$ Å. The other branch towards Thiele's ester is more problematic and it stops before reaching the
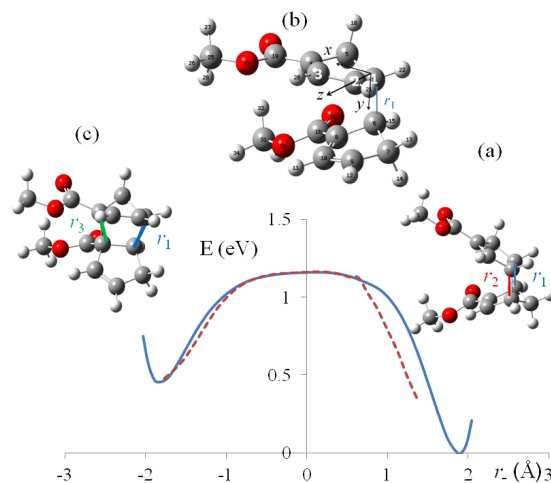

FIG. 1. Geometries of Thiele's ester (a), Cope transition state (b), and the product of the Cope rearrangement (c). Structures (a) and (c) are the initial and the target geometries. Full line: energy profile at the B3LYP DFT level along $r_- = r_3 - r_2$ obtained by varying r_2 or r_3 from the TS with optimization of all the other coordinates (RP1). Dashed line: intrinsic reaction path computed in mass-weighted coordinates (RP0). The z direction is fixed by the carbon atoms C_1 and C_2 in the upper ring of the TS structure which are the origin of the bonds r_1 and r_2, respectively. The x direction is in the plane $C_1 - C_2 - C_3$ where C_3 is the following C in the ring. The Ox direction is chosen for the laser control.

stationary point. However, this preliminary analysis reveals that in the TS region, the two main components of the IRC are the r_2 and r_3 coordinates. A first 1D model is a scan of r_2 or r_3 by steps of 0.5 Å up to 1.45 Å starting at the TS structure with optimization of all the other coordinates. The corresponding potential energy curve as a function of $r_- = r_3 - r_2$ is shown in full line in Fig. 1. This curve will be denoted RP1.

Next, a 2D minimum energy surface has been explored in a large range of r_2 and r_3 from 1.2 to 5.2 Å by steps of 0.1 Å. For large distances, the r_1 bond may break abruptly. Then, to obtain realistic walls as required for 2D dynamics which mainly explores the central region of the grid, most of the points of the upper corner have been optimized following r_2 and r_3 with an r_1 distance set at the value it has just before breaking, mainly in the range of 1.7 Å. Energy contours in the 2D potential energy and dipole moment surfaces are shown in Fig. 2. The *ab initio* points have been fitted by an analytical sum of products $V(r_2, r_3) = \sum_{i,j} c_{ij} r_2^i r_3^j$ and then transformed to the coordinates $r_- = r_3 - r_2$ and $r_+ = r_3 + r_2$. Fig. 2 also shows another 1D model denoted RP2, obtained from the 2D subspace only. RP2 is relatively close to the *ab initio* curve RP1. It is a polynomial fit imposing the steepest descent at the TS and the passage through the two minima. The different 1D potential energy and dipole moment curves are drawn in Fig. 3. The corresponding frequencies are, respectively, $\omega_{RP1} = 1027$ cm^{-1} and $\omega_{RP2} = 913$ cm^{-1}. We consider only the dipole component $\mu_x(r_-, r_+)$ having the strongest variation along r_-. The axes are defined in the inset of Fig. 1. $\mu_x(r_-, r_+)$ is the only component for which one can find a chain of matrix elements larger than 10^{-3} a.u. among the 2D vibrational states connecting the initial state to the target. The $\mu_x(r_-, r_+)$ component increases at the TS because the COO group is in the ring plane.
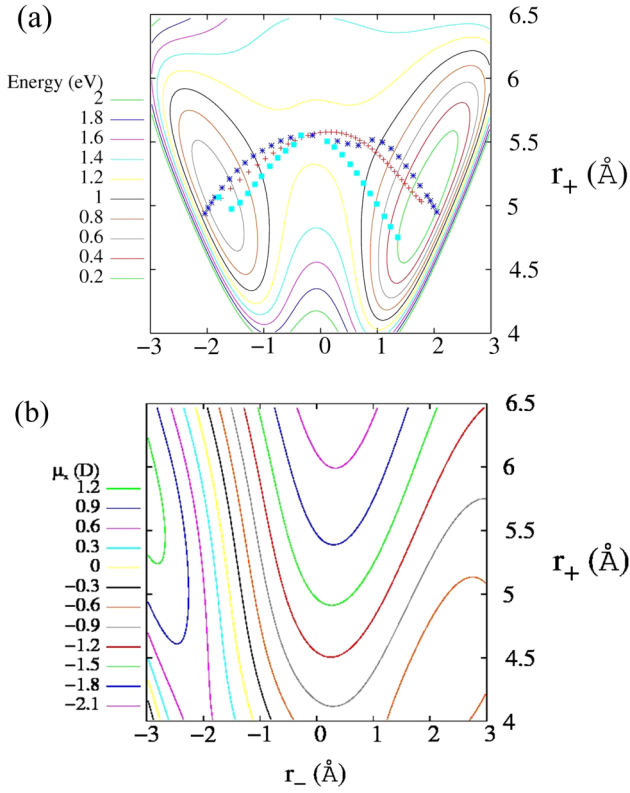
FIG. 2. Panel (a): contour plots in the B3LYP DFT 2D energy surface as a function of $r_- = r_3 - r_2$ and $r_+ = r_3 + r_2$ and different 1D reaction paths. Cyan squares: *ab initio* IRC, blue crosses: *ab initio* minimum energy path along r_2 or r_3 from the TS (RP1), red plus: polynomial fit connecting the minima and the TS with the steepest descent from the TS (RP2). Panel (b): contour plots in the dipole moment $\mu_x(r_-, r_+)$ for the chosen polarization. The axes are defined in Fig. 1.

We adopt a simple kinetic model. The coordinates r_2 and r_3 are treated as uncoupled Cartesian coordinates with a mass given by the reduced mass of a CC bond. After the linear combination $r_- = r_3 - r_2$ and $r_+ = r_3 + r_2$, the kinetic energy operator becomes $T_{r_-, r_+} = -(\hbar^2/2m)(\partial^2/\partial r_-^2 + \partial^2/\partial r_+^2)$ with $m = m_C/4$ and m_C is the mass of a C atom. The control consists in breaking r_2 and forming r_3 so that, for the 1D models, the reaction coordinate is described by r_- with the corresponding potential energy $V(r_-)$, and the kinetic energy operator is simply $T_{r_-} = -(\hbar^2/2m)\partial^2/\partial r_-^2$.

The laser field $E(t)$ is polarized linearly. The molecule is assumed to be aligned in the laboratory so that the Ox axis (see Fig. 1) coincides with the polarization axis. The subscript x is not indicated further for the field. The interaction is described at the dipolar approximation and the system Hamiltonian reads

$$H_S(t) = T_{\mathbf{r}} + V(\mathbf{r}) - \mu_x(\mathbf{r})E(t), \qquad (1)$$

where $\mathbf{r}$ is r_- or (r_-, r_+) for the 1D and 2D case, respectively.

When the system is coupled to a dissipative surrounding, we consider that only the coordinate r_- is coupled to a bath. The harmonic bath Hamiltonian is $H_B = 1/2 \sum_{i=1}^{N} (p_i^2/m_i + m_i \omega_i^2 q_i^2)$. The system-bath coupling $H_{SB} = -\sum_{i=1}^{N} c_i q_i r_-$ is bilinear and leads to a renormalization term $H_{ren} = K r_-^2/2$ with $K = \sum_{i=1}^{N} c_i^2/m_i \omega_i^2$. The coupling to the environment is described by the spectral density $J(\omega) = (\pi/2) \sum_i c_i^2/m_i \omega_i \, \delta(\omega - \omega_i)$
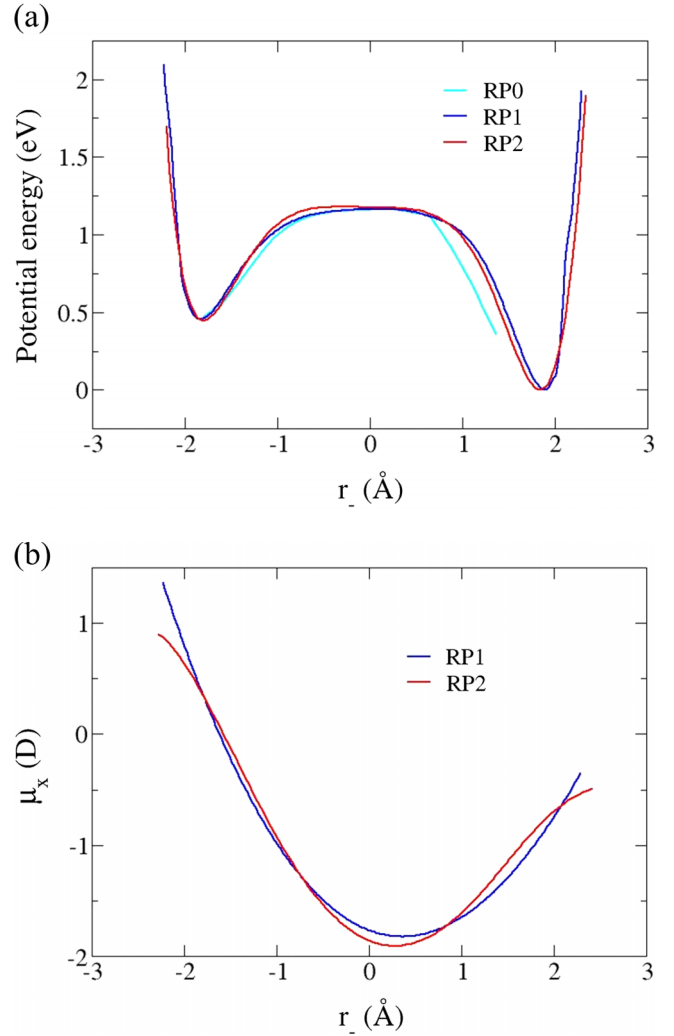

FIG. 3. Energy profile and dipole moment $\mu_x(r_-)$ of the different 1D paths.

which is taken here as an Ohmic function

$$J(\omega) = \lambda \omega e^{-\omega/\omega_c}. \qquad (2)$$

III. OPTIMAL CONTROL

The initial (ϕ_i) and target (ϕ_t) states are the ground vibrational states of the 1D RP1 or RP2 curves (Fig. 3(a)) or those of the two wells in the 2D case (Fig. 2(a)), corresponding to structures (a) and (c) of Fig. 1. The optimum field of duration t_f steers the initial state $\psi(t = 0) = \phi_i$ towards a final state $\psi(t_f)$ and the success is measured by the performance index $|\langle \psi(t_f) | \phi_t \rangle|^2$. In the Hilbert space, the OCT fields are obtained from the functional[22] built from this index, the constraint on the fluence, and the respect of the Schrödinger equation

$$J(\psi, \chi, E) = |\langle \psi(t_f) | \phi_t \rangle|^2 - \alpha \int_0^{t_f} \frac{E(t)^2}{s(t)} dt - 2\Re\Big(\langle \psi(t) | \chi(t) \rangle$$
$$\times \int_0^{t_f} \langle \chi(t) | \partial/\partial t + i\hbar H_S(t) | \psi(t) \rangle dt\Big),$$
$$(3)$$

where α and $\chi(t)$ are the Lagrange multipliers and $s(t) = \sin^2(\pi t/t_f)$ is an envelope assuring a smooth switch-off. The

variation according to the three variables leads to three coupled equations. The variation of χ leads to the Schrödinger equation for $\psi(t)$ with the initial condition $\psi(t=0) = \phi_i$. The variation of ψ gives the Schrödinger equation for $\chi(t)$ with the final condition $\psi(t = t_f) = \phi_t$, and finally, the variation according to E provides the expression of the optimum field

$$E(t) = -s(t)\Im(\langle\psi(t)\,|\,\chi(t)\rangle\langle\chi(t)|\mu_x|\psi(t)\rangle)/\alpha. \quad (4)$$

The equations are solved by the Rabitz monotonous algorithm.[22] At each iteration k, the field given by Eq. (4) is treated as a correction $\Delta E^{(k)}$ to the previous one so that the field is given by[62]

$$E^{(k)}(t) = E^{(k-1)}(t) + \Delta E^{(k)}(t). \quad (5)$$

In order to fix the integrated intensity to a given value $I_{max} = \int_0^{t_f} E(t)^2 dt$, α is not treated as an adjustable parameter as usually but it is computed at each iteration k by the relation[63]

$$\alpha^{(k)} = \left(\int_0^{t_f} E^{(k)}(t)^2 dt / I_{max}\right)^{1/2}. \quad (6)$$

When dissipation is involved, only the active coordinate r_- is coupled to the bath. In 1D simulations, we use the strategy developed in our previous work[54] where the Rabitz algorithm for the density matrix[64] has been coupled with the non-Markovian auxiliary matrix method.[55,56] This procedure becomes prohibitive in 2D when the number of states or grid points is large. We then use a Markovian approach[65,66] involving the propagation of a single matrix only.

As we impose a fixed integrated intensity I_{max} and a maximum absolute value of the field amplitude E_{max}, the exploration of the control landscape is restricted. Any initial guess does not necessarily lead to the perfect solution and the optimization may stop at a local maximum with a performance index lower than 100%.[67–72]

IV. RESULTS

The dissipative 1D model studied in our previous work[54] was the crudest way to account for the numerous atomic motions during the isomerization which mainly breaks r_2 and forms r_3. The reaction coordinate r_- was then coupled to a harmonic bath. Here, we extend the reactive subspace by including the coordinate r_+ which allows the exploration of the full r_2 and r_3 domain. The (r_-, r_+) coordinates are more appropriate than the (r_2, r_3) ones to compare with the 1D dynamics along r_-. The pulse duration is fixed to 15 ps and we impose a similar total integrated intensity $I_{max} = 3$ a.u. and a maximum absolute value of the field amplitude $E_{max} = 0.03$ a.u. (1.54×10^{10} Vm^{-1}).

The simulations were done using a time step of 0.19 fs and a spatial grid with 128 points for r_- and 64 points for r_+. The sampling is fixed according to the maximum kinetic energy in both directions. For simulations with dissipation, the temperature is fixed at $T = 300$ K and the spectral density cutoff is 1700 cm^{-1}. The friction coefficient λ [Eq. (2)] is reduced when passing from 1D ($\lambda = 8 \times 10^{-4}$ a.u.) to 2D ($\lambda = 6 \times 10^{-5}$ a.u.) and the values are calibrated to lead to an in-between

effect. We compare mechanisms induced by two 1D or two 2D fields only.

A. 1D optimized field as a guess for the 2D control

In this section, we examine to which extent a field optimized on a 1D path can be a good trial field for a control in the 2D subspace. We first optimize a field for the control along the 1D reaction paths RP1 and RP2 (see Fig. 2) without dissipation. They are denoted E_{RP1}^{1D} and E_{RP2}^{1D}. Both paths connect the TS and the minima but along slightly different curves in the (r_2, r_3) domain. The trial fields are chirped pulses of $t_f = 15$ ps given by $E(t) = E_{max} \cos(\omega(t)) \exp\left[-(t - t_{chirp})^2/2\sigma^2\right]$ with $\omega(t) = (\omega_1 + c(t - t_{chirp}))(t - t_{chirp})$ and $t_{chirp} = \frac{t_f}{2}$, $\sigma = 1.9$ ps and $c = 0.86$ ps^{-2}. The ω_1 frequency is ω_{RP1} (1027 cm^{-1}) or ω_{RP2} (913 cm^{-1}), i.e., the fundamental transition in the 1D model. In every 1D case, the performance index is 100% but falls to zero when the corresponding optimum fields drive the 2D process. A new optimization leading to the E_{RP1}^{2D} and E_{RP2}^{2D} fields is then performed by using the 1D E_{RP1}^{1D} and E_{RP2}^{1D} fields as trials. With the constraints of E_{max} and I_{max}, the success is then only of the order of 70%. Figure 4 compares the results obtained with the optimum E_{RP1}^{1D} and E_{RP2}^{1D} fields (blue dots) with those given by the E_{RP1}^{2D} and E_{RP2}^{2D} fields (red full lines) optimized with constraints. Panels (a) and (b) show the initial and target populations. In the 2D case, the excitation is faster but the localization towards the target begins later and remains incomplete. More insight about the barrier crossing dynamics can be seen in panels (c) and (d) by examining the occupation of all the delocalized states above the barrier. Obviously, the time spent in the delocalized states is clearly shorter by about a factor 2 in the 1D case. In 2D, the population in those states does not vanish at the end of the process, confirming that the final step is more difficult.

Figure 5 presents the mean position $\langle r_- \rangle$ (panels (a) and (b)) and the standard deviation $\sigma_{r_-} = \left(\langle r_-^2 \rangle - \langle r_- \rangle^2\right)^{1/2}$ (panels (c) and (d)) of the wave packet. Both observables show that the behavior in the initial well is very similar during the first 6 ps, but as soon as the wave packet reaches the flat barrier region, the delocalization of the 2D wave packet is more extensive and the control does not succeed in localizing it again, while the final $\langle r_- \rangle$ and σ_{r_-} are those of the target state in the 1D case. The total energy is drawn in panels (e) and (f). The maximum energy reached remains similar in 1D and 2D control showing again that it mainly depends on the time spent in the barrier region which is longer in the 2D case.

The spectrograms of the optimum fields are given in Figure 6. In the 1D case, one recognizes the fingerprint of the chirped trial field centered on the fundamental frequency ω_{RP1} (1027 cm^{-1}) or ω_{RP2} (913 cm^{-1}) of the RP1 or RP2 path, respectively. After the optimization, one observes that the frequencies involved in the first excitation step during the first 6 ps are quite similar for E_{RP1}^{2D} and its trial field E_{RP1}^{1D} or for E_{RP2}^{2D} and E_{RP2}^{1D}. On the contrary, the barrier crossing and the deexcitation require many more frequencies to try to localize the wave packet. The complexity of the field after 6 ps illustrates again that the difficult step concerns the dynamics through the quasi-continuum of delocalized states in the flat barrier region.
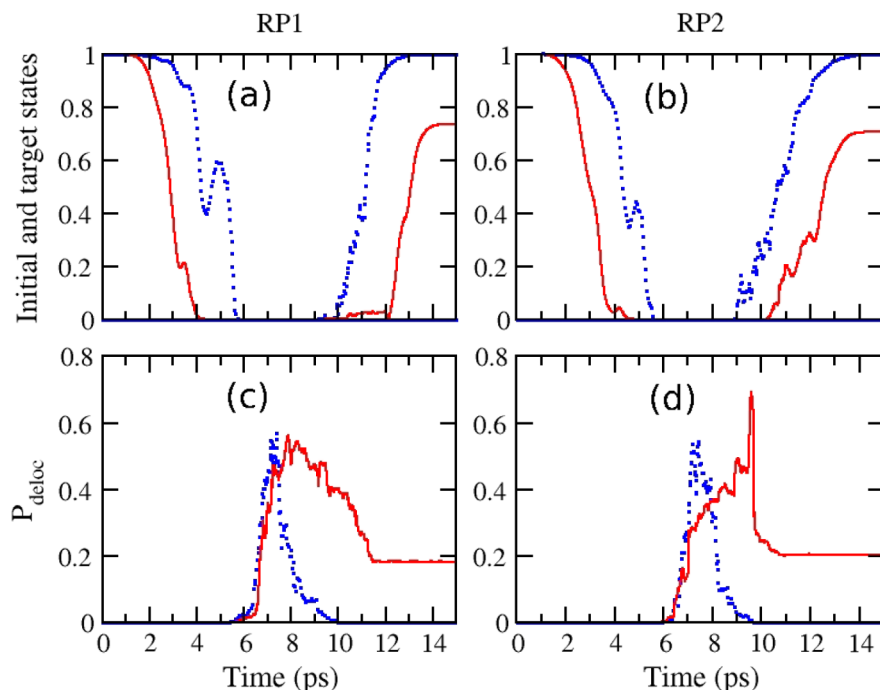
FIG. 4. Comparison of the population in the initial and target states (panels (a) and (b)) and in the delocalized states above the barrier (panels (c) and (d)) driven by the E_{RP1}^{1D} and E_{RP2}^{1D} fields for the 1D (blue dots) and by the E_{RP1}^{2D} and E_{RP2}^{2D} fields (full red lines). The RP1 and RP2 paths are shown in Figs. 2 and 3 and the spectrograms of the fields are compared in Fig. 6.

B. Comparison of 2D control strategies

As the optimum E_{RP1}^{1D} and E_{RP2}^{1D} fields generated by control along a reaction path are not efficient guess fields for optimization in 2D with fixed E_{max} and I_{max}, we first compare with a completely different strategy directly inspired by the properties of the 2D subspace. Next, we compare the robustness of the different 2D controlled dynamics against dissipation. A new iterative optimization with non-Markovian dissipation is unfeasible with the large density matrices of

the 2D case (either grids of 64 and 128 points for r_+ and r_- or 1500 vibrational states in the eigen basis set). We prepare three guess fields of 5 ps for a three step strategy with intermediary doorway states. The $\mu_x(r_-, r_+)$ function allows us to find a chain of eigenstates coupled by dipolar couplings larger than 10^{-3} a.u. connecting the initial state to the target via one of the first delocalized states. These states are represented in Fig. 7. The first step is the excitation to a highly excited state in the initial well (state 174). The third one is the deexcitation from one excited vibrational state of the product well (state
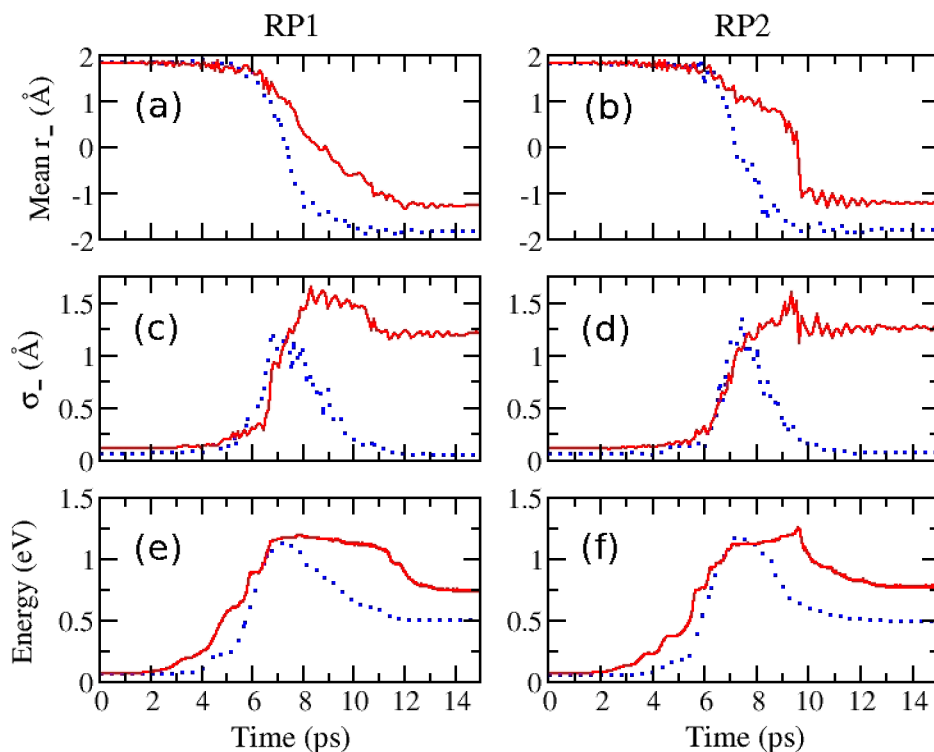

FIG. 5. Comparison of the mean r_- position (panels (a) and (b)), the standard deviation σ_- (panels (c) and (d)), and total energy (panels (e) and (f)) of the wave packet driven by the E_{RP1}^{1D} and E_{RP2}^{1D} fields (blue dots) and by the E_{RP1}^{2D} and E_{RP2}^{2D} fields (full red lines). The RP1 and RP2 paths are shown in Figs. 2 and 3 and the spectrograms of the fields are compared in Fig. 6.
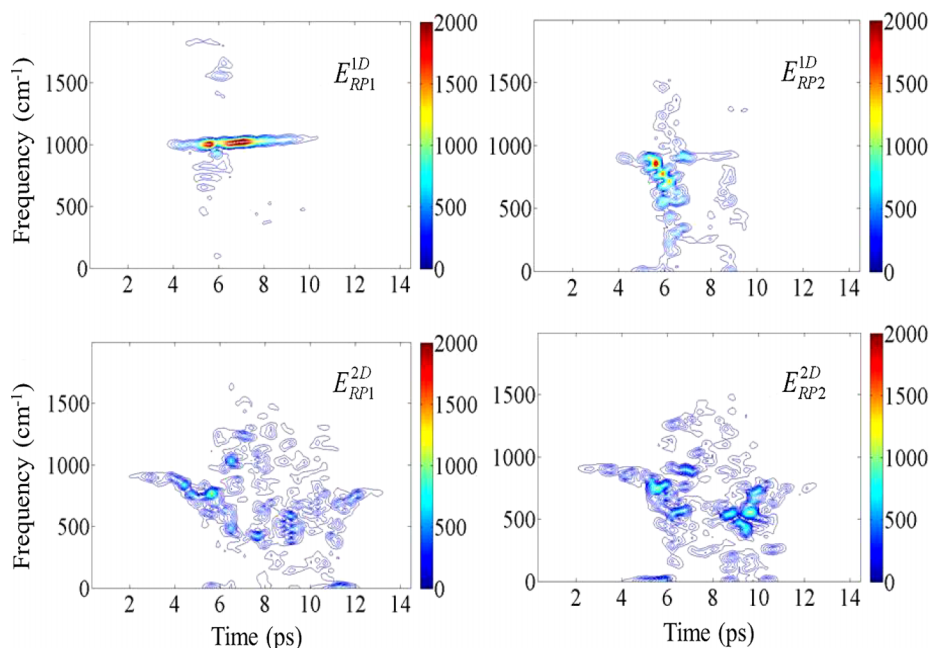
FIG. 6. Spectrograms of the optimum fields. The E_{RP1}^{1D} and E_{RP2}^{1D} fields drive the control along the RP1 and RP2 paths (see Fig. 2) with a chirped trial pulse. The E_{RP1}^{2D} and E_{RP2}^{2D} fields are optimized with the trial fields E_{RP1}^{1D} and E_{RP2}^{1D}. The maximal amplitude of the fields is fixed to $E_{max} = 0.03$ a.u. and the integrated intensity $I_{max} = 3$ a.u. The color code for the intensity of the Fourier transform is given in arbitrary units similar for the two cases.

211) to the target state (state 36). The trial fields contain all the selected frequencies for the ladder climbing or down. For the second step of the barrier crossing, the guess field is formed by the two frequencies connecting the states 174 and 211 through a common intermediary low lying delocalized state (state 310). This transition from state 174 to state 211 through state 310 is in the spirit of a STIRAP[73,74] (Stimulated Raman adiabatic process) but the duration of the corresponding pulse is too short and a STIRAP pulse optimized on the three-state subspace is not appropriate due to the high density of delocalized states in the 2D model. Similarly, the use of all the intermediary transition frequencies in the ladder climbing and down is inspired from the N-level STIRAP generalization but the adiabatic conditions are not fulfilled here.[75] These three fields are optimized up to about 80% and then concatenated to become the guess field for the OCT with the same constraints E_{max} and I_{max} as before. This strategy leads to a field E_{3steps}^{2D}

providing a performance index of 98% so the OCT converges in spite of the constraints. This 3-step approach is merely in the spirit of a well-known strategy in which existing knowledge should be incorporated into the control (e.g., the passage across a transition state, etc.). The control objective can then be broken down into time intervals, each of which being optimized by OCT.[76]

Fig. 8 shows the spectrogram of the E_{3steps}^{2D} field. One recognizes the main guess frequencies used during the three steps. The excitation involves mainly the frequencies inducing the 2-4 (526 cm^{-1}), 4-8 (538 cm^{-1}), and 8-16 (831 cm^{-1}) climbing. The OCT finds more frequencies than the two guess ones (310-174, 1800 cm^{-1} and 310-211, 1200 cm^{-1}) during the TS crossing. Finally, the deexcitation clearly uses the ladder down during the last five ps (mainly 123-83, 970 cm^{-1}; 83-36, 850 cm^{-1}; 56-42, 552 cm^{-1}) and at the end of the control, the final transition 42-36 (271 cm^{-1}) towards the target appears.
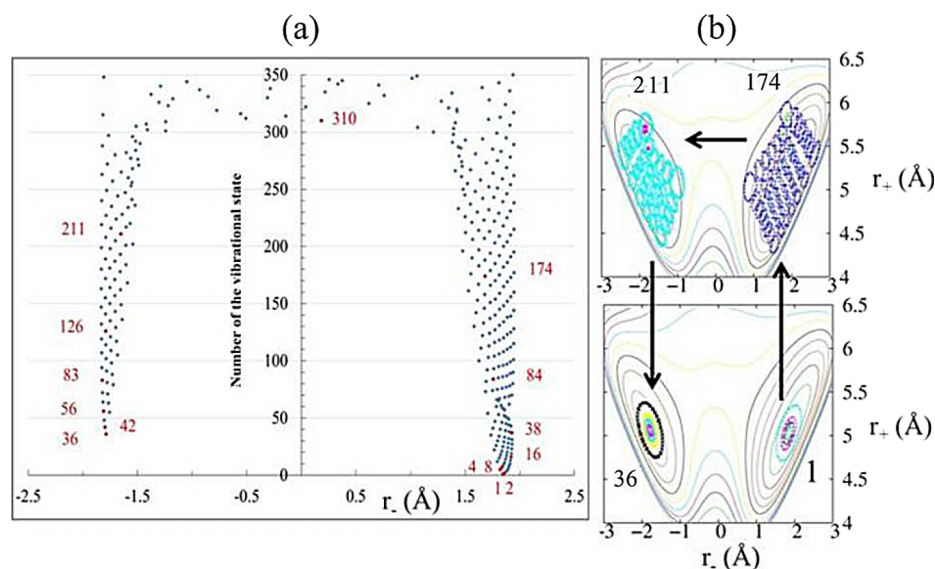

FIG. 7. Panel (a): mean position of the 2D eigenstates up to the first delocalized states. The intermediary states used in the guess fields are shown in red. These states are connected by a transition dipole larger than 10^{-3} a.u. The guess frequencies are those corresponding to the ladder climbing between the selected states. Panel (b): contour plots in the initial and target wells and in the vibrational doorway states chosen for the excitation and deexcitation steps.
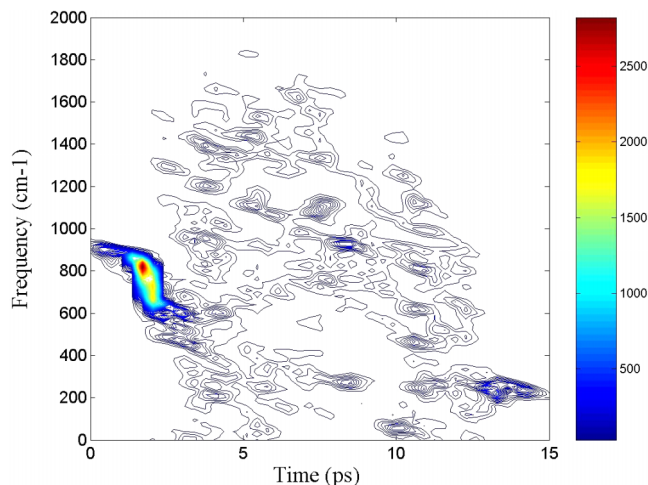
FIG. 8. Spectrogram of the E_{3steps}^{2D} field. The guess frequencies are those of the ladder climbing and down represented in Fig. 7. The color code for the intensity of the Fourier transform is given in arbitrary units similar to that of Fig. 6.

The full blue curves in Figure 9 compare the dynamics driven by the OCT fields E_{3steps}^{2D} and E_{RP1}^{2D} obtained in Sec. IV A. Panels (a) and (b) show that the final deexcitation is quasi complete in the three-step strategy. Similarly, panels (c) and (d) show that the delocalized states are almost completely depopulated with E_{3steps}^{2D} while it is not the case with E_{RP1}^{2D}. A striking difference is observed when we analyze only the population in the very highly excited states above the barrier, starting from about 1.5 eV (see panels (e) and (f) in Fig. 9). While the E_{RP1}^{2D} field excites these very high lying states, in the case of the three-step strategy, these states are hardly populated at all. This is a direct consequence of the guess field focusing on the $v = 174$ and $v = 211$ states as "doorway" states and

suggesting the transition through the lowest delocalized state above the barrier.

Before discussing the effect of decoherence below, we want to examine the average positions of the driven wave packets. Figure 10 shows contour plots in the potential energy surface and the blue crosses follow the RP1 path. The red plus signs are the averages $\langle r_- \rangle$ and $\langle r_+ \rangle$ along the controlled trajectory. The early excitation is very similar in both cases. Obviously, the mean trajectory followed with E_{RP1}^{2D} deviates from the proposed 1D path. The localization in the final well is more completely achieved by the E_{3steps}^{2D} field which induces the ladder down from the vibrational doorway state.

The last point of this section addresses again the robustness of a field against dissipation. It has not been possible to optimize an OCT field in the non-Markovian approach in this example due to the dimension of the grids. We only compared the Markovian dynamics driven by the E_{RP1}^{2D} and E_{3steps}^{2D} fields when the system is coupled to an Ohmic bath. Red dotted lines in Figure 9 show the result of this dissipative dynamics. Even if the occupation of the delocalized states is quite similar in this example (see panels (c) and (d) in Fig. 9), it is a little bit more extensive with the E_{3steps}^{2D} field and the previous observation is qualitatively confirmed. The drop in yield is larger for the E_{3steps}^{2D} field (panel (b) in Fig. 9) than for the E_{RP1}^{2D} field (panel (a) in Fig. 9). Decoherence destroys the mechanism ensuring a good deexcitation and one observes an increase of population in the highly excited delocalized states.

C. Coupling the 1D path to a bath or an active mode

Finally, we compare the controlled dynamics when the r_- coordinate is coupled to a dissipative bath or to the second main active mode. Even if the main reactive coordinate during the
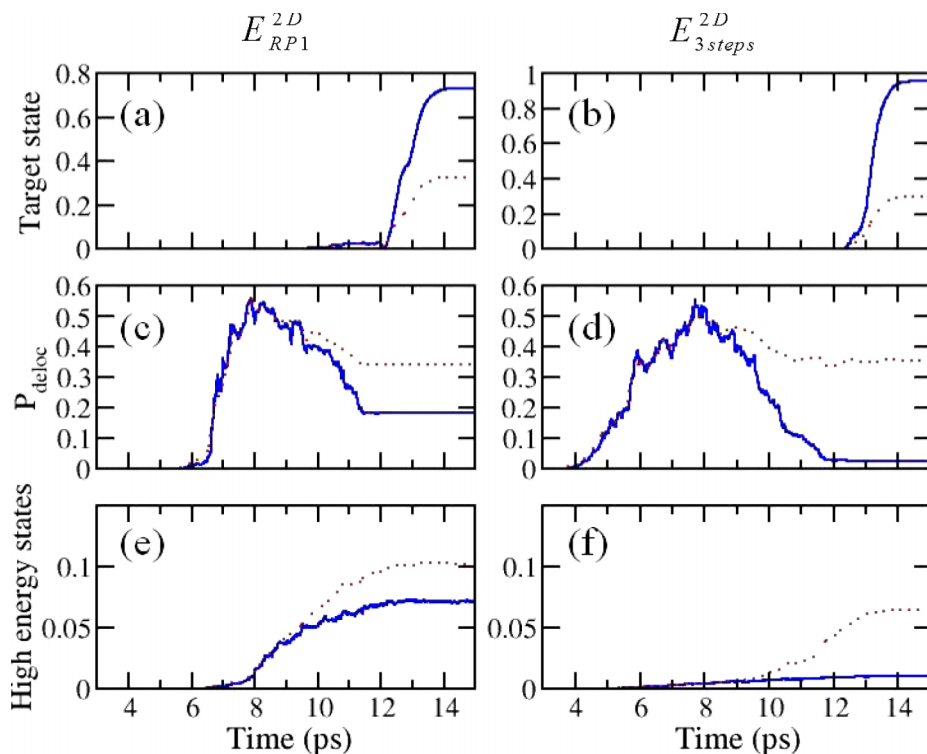

FIG. 9. Comparison of the dynamics driven by the E_{RP1}^{2D} and E_{3steps}^{2D} fields without dissipation (full blue lines) and with dissipation (red dotted line) ($\lambda = 6 \times 10^{-5}$ a.u. [Eq. (2)], $\omega_c = 1700$ cm^{-1}, $T = 300$ K). Upper panels: population in the target state; middle panels: total population in the delocalized states above the barrier; lower panels: population in the high energy states above the barrier in the [1.5, 1.9] eV range.
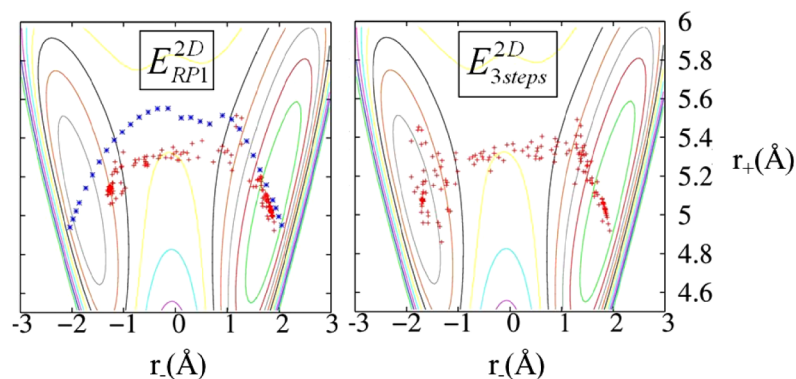
FIG. 10. Spots of the average position ($\langle r_- \rangle$, $\langle r_+ \rangle$) of the wave packet driven by the E_{RP1}^{2D} and E_{3steps}^{2D} fields in the 2D subspace. Red plus signs: average position in the 2D plane, blue crosses: *ab initio* minimum energy path from the TS (RP1) (see Fig. 2).

isomerization is r_-, we find that the control must account for the other modes. Here, we compare the controlled dynamics for two models where r_- is coupled either to a dissipative bath mimicking the ensemble of the remaining molecular modes ((r_-, *bath*) model) or to the second main mode r_+ ((r_-, r_+) model). As discussed in our previous work,[54] in the dissipative case, the control does not directly act on the bath modes and the remarkable result was that to fight dissipation the control decreases the time spent in the delocalized states along the active coordinate. On the contrary, in the (r_-, r_+) model, the E_{3steps}^{2D} field leads to the target populating the delocalized states during a longer time. The control now exploits the vibrational component along r_+ and the dipolar coupling among 2D eigenstates to achieve the deexcitation.

In the (r_-, *bath*) model, we first illustrate again the reduction of the barrier crossing timescale in the dissipative 1D control. Figure 11 compares the dynamics driven by the E_{RP1}^{1D} field (see Fig. 6 for the results without dissipation) when r_- is coupled to the bath (blue lines) and that driven by a control field optimized in the presence of dissipation denoted $E_{RP1}^{1D-diss}$ (red lines). One sees the notable decrease of the yield provided by E_{RP1}^{1D} due to dissipation since the final target population drops from 100% to 18%. The $E_{RP1}^{1D-diss}$ field finds a new mechanism and increases the population to 68%. The modification of the

dynamics mainly concerns the duration of the TS crossing as can be seen in panel (c) from the population in the delocalized states, in panel (b) from the variation of the deviation σ_{r_-}, and in panel (d) from the mean r_- position. The same dynamical observables relative to the (r_-, r_+) model are presented in cyan dashed lines in Figure 11. The target state population (panel (a)) shows that the control is very good with the field E_{3steps}^{2D}. However, the mechanism is completely different. One sees in panel (c) that the delocalized states are more populated than in the previous case. The delocalization (panel (b)) is larger during the excitation and the TS crossing but the deexcitation is more efficient.

The decoherence of the dynamics along r_- in both models is now compared by the corresponding reduced density matrices which are $\rho_S(t)$ in the (r_-, *bath*) case and $\rho_{r_-}(t) = Tr_{r_+}(\rho_S(t))$ in the (r_-, r_+) model. Figure 12 shows the purity, i.e., $Tr(\rho_S^2(t))$ (panel (a)) and $Tr(\rho_{r_-}^2(t))$ (panel (b)), respectively. In the (r_-, *bath*) case, the initial value is 1 since the initial 1D state is a pure case because the frequency ω_{RP1} (1027 cm^{-1}) is larger than $k_B T$ at room temperature such that the Boltzmann population of the ground state is 1.

Decoherence begins when the system is in the delocalized states in the TS region. The monotonous decrease of $Tr(\rho_S^2(t))$ towards an asymptotic value different from 1 shows that the
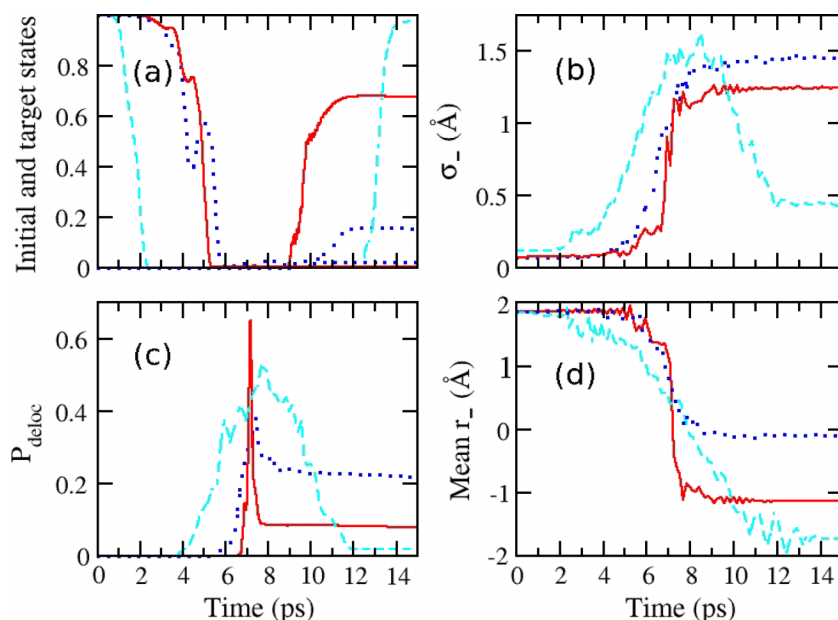

FIG. 11. Characteristics of the controlled dynamics in the (r_-, *bath*) or (r_-, r_+) models. Blue dots: dynamics driven by E_{RP1}^{1D} in the presence of dissipation ($\lambda = 8 \times 10^{-4}$ a.u. [Eq. (2)], $\omega_c = 1700$ cm^{-1}, $T = 300$ K), full red lines: control with $E_{RP1}^{1D-diss}$, dashed cyan lines: control with E_{3steps}^{2D}. Panel (a): initial and target state populations; panel (b): standard deviation σ_-; panel (c): population in the delocalized states; panel (d): average position $\langle r_- \rangle$.
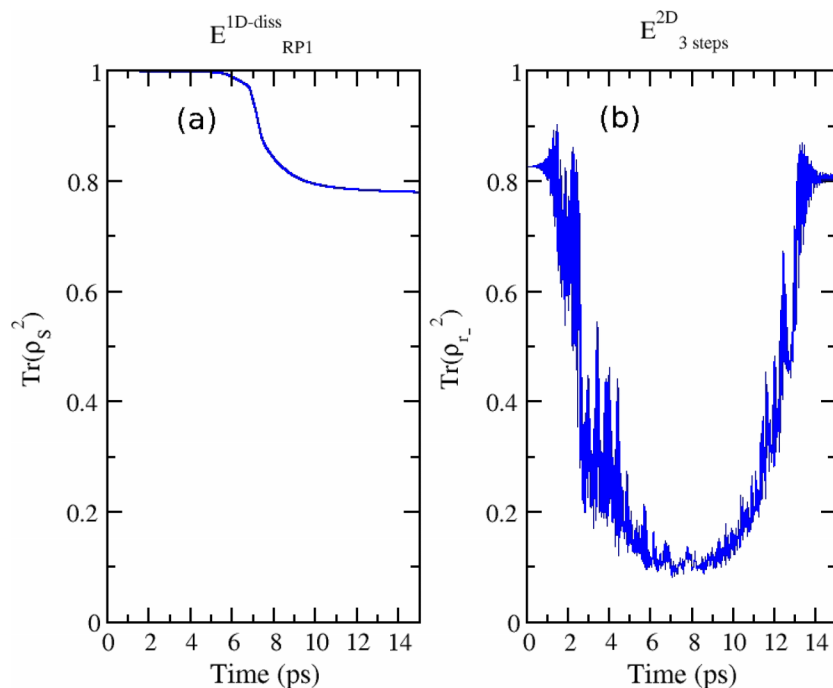
FIG. 12. Purity of the reduced dynamics along the reactive coordinate r_-. Panel (a): $Tr\left(\rho_S^2(t)\right)$ when the driving field is $E_{RP1}^{1D-diss}$ ($\lambda = 8 \times 10^{-4}$ a.u. [Eq. (2)]); panel (b): $Tr\left(\rho_{r_-}^2(t)\right)$ with field E_{3steps}^{2D}.

control cannot completely form the pure 1D target state. Note that this limiting value obviously depends on the value of the friction λ chosen in the Ohmic spectral density. In the (r_-, r_+) model, the behavior is different. The initial or target values of $Tr\left(\rho_{r_-}^2(t)\right)$ are fixed by the corresponding vibrational states which are not separable in the (r_-, r_+) space (see Fig. 7). During the evolution, $Tr\left(\rho_{r_-}^2(t)\right)$ first decreases due to the strong correlation between the modes. During the deexcitation, $Tr\left(\rho_{r_-}^2(t)\right)$ regularly increases towards the limiting value of the target. The second r_+ mode does not act as a bath and the correlation is plainly used by the control.

V. CONCLUDING REMARKS

The role of the active subspace dimension in simulations of quantum control remains an open question. We have addressed here a particular point: what is the response of the control field when a one-dimensional reaction path is coupled to an inactive dissipative bath or to a second active mode? In this work, we have presented optimal control simulations of the Cope rearrangement of Thiele's ester (methyl-cyclopentadienenylcarboxylate dimer). Even though the controlled geometrical rearrangement can mainly be described by a 1D reaction path with the difference of the r_2 and r_3 distances being the reaction coordinate (see Fig. 1), other geometrical deformations are at play and their dynamics modifies the control scenario. To account for these additional deformations in the context of coherent control, we have analyzed two cases, which can be seen as limiting cases: in one model, the remaining modes are considered as a dissipative bath, to which the reaction coordinate is coupled, and in the other, we include explicitly a second degree of freedom in the control dynamics. These two models are thus two cases of a general strategy, in which the full space of molecular deformations is partitioned into a subspace of strongly affected deformations, and a remaining one which

can be treated at a more approximate level as a thermal bath. If the dynamics includes the two-dimensional space, accounting for the dipole components in both dimensions, the control algorithm can profit from this higher dimensionality to find efficient pathways. On the other hand, the modes treated as a thermal bath cannot be actively driven by the control fields, but act as a source of decoherence, which hampers the control scenario.

As a main result, we have shown how the control remarkably adapts to these two different situations: in the 2D case, the second included mode is actively excited by the control pulse, leading to a more efficient deexcitation to the target, and thus to a higher control yield. In the dissipative case, this is not possible, and to optimize the yield, the control algorithm converges to fields which significantly accelerate the passage across the transition state, thus minimizing the decoherence. It has not been possible to optimize a field in a 2D dissipative dynamics in order to verify our conclusion. However, the robustness of the fields optimized by the 2D control against decoherence described by a Markovian master equation confirms the expected behavior: decoherence mainly affects the dynamics in the delocalized states.

To conclude, our work shows that a careful modeling and a thorough partitioning into system and bath is required for realistic control calculations of complex, multidimensional reactions. Specifically, the choice of the active modes should not only be based on the Hamiltonian but also on the multidimensional dipole function, which determines to which extent an external field can excite specific modes. Even though a full dimensional quantum treatment would be preferable, for example, by the MCTDH method,[34,37,38] very often, this is still not feasible, due to lack of relevant potential and dipolar moment surfaces, and one needs to revert to a modeling by reduced dynamics. Subsequent control calculations could then find efficient schemes, which use the multidimensional dynamics and react to the bath-induced decoherence. While

in this work, we focused on a density matrix formalism when modeling the environment, a stochastic approach in the Hilbert space, which mimics the surrounding by a fluctuating force is an interesting perspective, in particular, in the context of coherent control.[77,78] Future work will be directed along these lines.

ACKNOWLEDGMENTS

[1] S. Rice and M. Zhao, *Optimal Control of Molecular Dynamics* (Wiley, New York, 2003).

[2] M. Shapiro and P. Brumer, *Principles of Quantum Control of Molecular Processes* (Wiley, New York, 2003).

[3] D. Tannor and S. A. Rice, J. Chem. Phys. **83**, 5013 (1985).

[4] R. Kosloff, S. Rice, P. Gaspard, S. Tersigny, and D. Tannor, Chem. Phys. **139**, 201 (1989).

[5] S. Shi and H. Rabitz, J. Chem. Phys. **92**, 364 (1989).

[6] P. Brumer and M. Shapiro, Annu. Rev. Phys. Chem. **4**, 257 (1992).

[7] C. Brif, R. Chakrabarti, and H. Rabitz, New J. Phys. **12**, 075008 (2010).

[8] A. Präkelt, M. Wollenhaupt, A. Assion, C. Horn, C. Sarpe-Tudoran, M. Winter, and T. Baumert, Rev. Sci. Instrum. **74**, 4950 (2003).

[9] Z. Jiang, C. B. Huang, D. E. Leaird, and A. M. Weiner, J. Opt. Soc. Am. B **24**, 2124 (2007).

[10] D. Strasfeld, S. H. Shim, and M. T. Zanni, Phys. Rev. Lett. **99**, 038102 (2007).

[11] G. Vogt, G. Krampert, P. Niklaus, P. Nuernberger, and G. Gerger, Phys. Rev. Lett. **94**, 068305 (2005).

[12] G. Vogt, P. Nuernberger, T. Brixner, and G. Gerber, Chem. Phys. Lett. **433**, 211 (2006).

[13] V. I. Prokhorenko, A. M. Nagy, L. S. Brown, and R. J. Dwayne Miller, Chem. Phys. **341**, 296 (2007).

[14] A. Assion, T. Baumert, M. Bergt, T. Brixner, B. Kiefer, V. Seyfried, M. Strehle, and G. Gerber, Science **282**, 151 (1998).

[15] D. Sofikitis, S. Weber, A. Fioretti, R. Horchani, M. allegrini, B. Chatel, D. Comparat, and P. Pillet, New J. Phys. **11**, 055037 (2009).

[16] C. Horn, M. Wollenhaupt, M. Krug, T. Baumert, R.de Nalda, and L. Bañares, Phys. Rev. A **73**, 031401 (2006).

[17] J. Vala, Z. Amitay, B. Zhang, S. Leone, and R. Kosloff, Phys. Rev. A **66**, 62316 (2002).

[18] L. Znakovskaya, P. von den Hoff, S. Zherebtsov, A. Wirth, O. Herrwerth, M. Vrakking, R. de Vivie-Riedle, and M. F. Kling, Phys. Rev. Lett. **103**, 103002 (2009).

[19] A. E. Bryson and Y.-C. Ho, *Applied Optimal Control* (Taylor & Francis, New York, London, 1975).

[20] T. E. Skinner, T. O. Reiss, B. Luy, N. Khaneja, and S. J. Glaser, J. Magn. Reson. **163**, 8 (2003).

[21] J. Somlói, V. A. Kazakovski, and D. J. Tannor, Chem. Phys. **172**, 85 (1993).

[22] W. Zhu, J. Botina, and H. Rabitz, J. Chem. Phys. **108**, 1953 (1997).

[23] W. Zhu and H. Rabitz, J. Chem. Phys. **109**, 385 (1998).

[24] Y. Maday and G. Turinici, J. Chem. Phys. **118**, 8191 (2003).

[25] L. González, D. Kroner, and I. Sola, J. Chem. Phys. **115**, 2519 (2001).

[26] M. Artamonov, T.-S. Ho, and H. Rabitz, J. Chem. Phys. **124**, 064306 (2006).

[27] V. May, D. Ambrosch, M. Oppel, and L. González, J. Chem. Phys. **127**, 144102 (2007).

[28] Y. Kurosaki, M. Artamonov, T.-S. Ho, and H. Rabitz, J. Chem. Phys. **131**, 044306 (2009).

[29] Y. Kurosaki, T.-S. Ho, and H. Rabitz, J. Chem. Phys. **140**, 084305 (2014).

[30] D. Geppert, A. Hofmann, and R. de Vivie-Riedle, J. Chem. Phys. **119**, 5901 (2003).

[31] M. Abe, Y. Ohtsuki, Y. Fujimura, and W. Domcke, J. Chem. Phys. **123**, 144508 (2005).

[32] D. Sugny, C. Kontz, M. Ndong, Y. Justum, G. Dive, and M. Desouter-Lecomte, Phys. Rev. A **74**, 043419 (2006).

[33] M. Abe, Y. Ohtsuki, Y. Fujimura, Z. Lan, and W. Domcke, J. Chem. Phys. **124**, 224316 (2006).

[34] M. Schröder, J.-L. Carreón-Macedo, and A. Brown, Phys. Chem. Chem. Phys. **10**, 850 (2008).

[35] C. Gollub, M. Kowalewski, S. Thallmair, and R. de Vivie-Riedle, Phys. Chem. Chem. Phys. **12**, 15780 (2010).

[36] C.-C. Shu, T. Rozgonyi, L. González, and N. E. Henriksen, J. Chem. Phys. **136**, 174303 (2012).

[37] L. Wang, H.-D. Meyer, and V. May, J. Chem. Phys. **125**, 014102 (2006).

[38] G. A. Worth and C. Sanz Sanz, Phys. Chem. Chem. Phys. **12**, 15570 (2010).

[39] N. Dolic, K. Sundermann, L. González, O. Mo, J. Giraud-Girard, and O. Kühn, Phys. Chem. Chem. Phys. **1**, 1247 (1999).

[40] A. Kuhl and W. Domcke, Chem. Phys. **259**, 227 (2000).

[41] O. Kühn, J. Phys. Chem. A **106**, 7671 (2002).

[42] O. Kühn and H. Naundorf, Phys. Chem. Chem. Phys. **5**, 79 (2003).

[43] K. Hoki and P. Brumer, Phys. Rev. Lett. **95**, 168305 (2005).

[44] W. Zhu and H. Rabitz, J. Chem. Phys. **118**, 6751 (2003).

[45] F. Shuang and H. Rabitz, J. Chem. Phys. **124**, 154105 (2003).

[46] S. Beyvers, Y. Ohtsuki, and P. Saalfrank, J. Chem. Phys. **124**, 234706 (2006).

[47] F. Caruso, S. Montangero, T. Calarco, S. F. Huelga, and M. B. Plenio, Phys. Rev. A **85**, 042331 (2012).

[48] M. V. Korolkov, J. Manz, and G. K. Paramonov, J. Chem. Phys. **105**, 10874 (1996).

[49] Y. Ohtsuki, J. Chem. Phys. **119**, 661 (2003).

[50] R. Xu, Y. Yan, Y. Ohtsuki, Y. Fujimura, and H. Rabitz, J. Chem. Phys. **120**, 6600 (2004).

[51] D. Sugny, M. Ndong, D. Lauvergnat, Y. Justum, and M. Desouter-Lecomte, J. Photochem. Photobiol., A **190**, 359 (2007).

[52] R. Xu, Y. J. Yan, Y. Ohtsuki, Y. Fujimura, and H. Rabitz, J. Chem. Phys. **120**, 6600 (2004).

[53] G. Dive, R. Robiette, A. Chenel, M. Ndong, C. Meier, and M. Desouter-Lecomte, Theor. Chem. Acc. **131**, 1236 (2012).

[54] A. Chenel, G. Dive, C. Meier, and M. Desouter-Lecomte, J. Phys. Chem. A **116**, 11273 (2012).

[55] C. Meier and D. J. Tannor, J. Chem. Phys. **111**, 3365 (1999).

[56] A. Pomyalov, C. Meier, and D. J. Tannor, Chem. Phys. **370**, 98 (2010).

[57] S. P. Shah and S. A. Rice, J. Chem. Phys. **113**, 6536 (2000).

[58] A. D. Becke, J. Chem. Phys. **98**, 5648 (1993).

[59] M. J. Frisch *et al.*, Gaussian 09, Revision A1 (Gaussian, Inc., Wallingford, CT, 2009).

[60] J. Thiele, Ber Dtsch. Chem. Ges. **34**, 68 (1901).

[61] A. Marchand, D. Zhao, T. Ngooi, and V. Vidyasagar, Tetrahedron **49**, 2613 (1993).

[62] J. P. Palao and R. Kosloff, Phys. Rev. Lett. **89**, 188301 (2002).

[63] J. Werschnik and E. K. U. Gross, J. Phys. B: At., Mol. Opt. Phys. **40**, 175 (2007).

[64] Y. Ohtsuki, W. Zhu, and H. Rabitz, J. Chem. Phys. **110**, 9825 (1999).

[65] V. May and O. Kühn, *Charge and Energy Transfer in Molecular System* (Wiley-VCH, Berlin, 2011).

[66] P. Gaspard and M. Nagaoka, J. Chem. Phys. **111**, 5668 (1999).

[67] H. Rabitz, M. Hsieh, and C. Rosenthal, J. Chem. Phys. **124**, 204107 (2006).

[68] R. Wu, A. Pechen, H. Rabitz, M. Hsieh, and B. Tsou, J. Math. Phys. **49**, 022108 (2008).

[69] M. Hsieh, R. Wu, and H. Rabitz, J. Chem. Phys. **130**, 104109 (2009).

[70] K. W. Moore and H. Rabitz, J. Chem. Phys. **137**, 134113 (2012).

[71] A. P. Pechen and D. J. Tannor, Phys. Rev. Lett. **106**, 120402 (2011).

[72] A. Donovan, B. Beltrani, and H. Rabitz, Chem. Phys. **425**, 46 (2013).

[73] T. Hellmann and K. Bergmann, J. Chem. Phys. **104**, 7068 (1996).

[74] K. Bergmann, H. Theuer, and B. W. Shore, Rev. Mod. Phys. **70**, 1003 (1998).

[75] V. S. Malinovsky and D. J. Tannor, Phys. Rev. A **56**, 4929 (1997).

[76] S. Beyvers and P. Saalfrank, J. Chem. Phys. **128**, 074104 (2008).

[77] G. Füchsel, T. Klamroth, J. C. Tremblay, and P. Saalfrank, Phys. Chem. Chem. Phys. **12**, 14082 (2010).

[78] J. C. Tremblay, J. Chem. Phys. **134**, 174111 (2011).